A General Approach to Programmable and Reconfigurable Emulation of Power Impedances

***Abstract*— Starting with a brief review on existing methods of impedance emulation, this paper addresses a general and systematic approach to programmable and reconfigurable emulation of power impedances. The proposed approach not only enables the impedance value to be programed, it also allows the characteristics (i.e. type) of the impedance to be reconfigured instantly during operation. Based on the proposed control method, emulation of at least six types of emulated power impedances (EPI) can be easily attained. In particular, it is theoretically and practically demonstrated that the impedance characteristic can be emulated through a combination of different functions. The systematic derivation of these functions is explained. New techniques that compensate the circuit power losses are introduced. This general approach has been practically verified in several EPI. Both steady-state and dynamic performance of these EPI confirm the programmability and re-configurability. It is envisaged that the proposed method can be applied to a range of functions such as power filtering, energy storage and even power conversion based on direct impedance control.**

I. INTRODUCTION

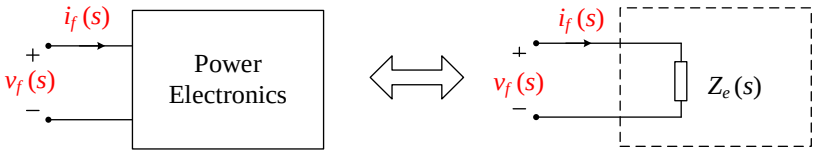

Fig. 1. An emulated power impedance $Z_e(s)$ based on power electronics.

An emulated power impedance (EPI) is a two-terminal power-electronic device that can actively mimic the exact voltage-current characteristic of a physical passive component (Fig.1). The basic principle of an EPI is to control the power electronics such that its terminal current i_f and terminal voltage v_f satisfy

$$i_f(s) = \frac{v_f(s)}{Z_e(s)}, \tag{1}$$

where $Z_e(s)$ is the transfer function that defines the characteristic impedance in the s domain.

The concept of EPI is not new. The early attempt to use an EPI can be traced back to the input current shaper for active power factor correction applications in the early 1900's, where the power converter turns its

associated load into an emulated resistor [1]. Over the past years, the concept of EPI is quickly evolving and has been widely employed for many power electronics and power system applications. One immediate application is to directly replace physical power impedances, because an EPI built from advanced semiconductors and control techniques can be made more compact, lightweight [2]–[4], (possibly) more reliable [5], [6], and being capable of adjusting its impedance value [4], [7]–[9]. For instance, an emulated inductor has been reported as a direct replacement of the heavy dc-link inductor for adjustable speed drive applications [4] and a variable line impedance emulator for hardware-in-the-loop applications [7]. An emulated capacitor has been used to replace the unreliable dc-link capacitors [2] and to stabilize the distributed DC power supply system [8]. Another major application of EPI is to provide power flow control and ancillary services, such as active power filtering and var compensation for power system application [9]–[11]. It has been demonstrated that the control structure of an EPI can be simpler than that of the existing control methods. Presently, an EPI can only be designed to perform a single task because it can only emulate a fixed type of impedance at a time. As a result, the potential of EPI is somehow constrained. One example is the use of EPI as a static var compensator (SVC). Reported EPI can only generate capacitive or inductive reactive power because of its inability to interchange between a capacitive and an inductive mode of operation. In this case, a programmable EPI (of which not only the value of its impedance but also its type can be easily reconfigured) will be highly desirable for achieving a true SVC, through which both types of reactive power can be generated. A programmable EPI may also be useful as a multi-functional equipment of which the functions can be conveniently defined by users according to the required tasks. Although it has been predicted in theory that any EPI can be synthesized based on (1) [12], the issues and solutions towards achieving a practical programmable EPI have never been reported in prior arts.

In this paper, the programmable and re-configurable aspects of a general EPI are systematically examined and explored. The objective is to identify and resolve the technical issues towards a general and re-configurable impedance emulation method. According to [12], the emulation of a general impedance requires a minimum of two power converters (one for programming input voltage and current relationship,

and the other for balancing active and reactive power). For illustration purposes, only a programmable and re-configurable power reactance is constructed to prove the concept. Since no real power generation is needed (theoretically), only one power converter can be employed if the output termination is chosen appropriately to facilitate power balance. This makes the characterization (such as the control method, the bandwidth) of an EPI easier. In Section II, existing EPI technologies for emulating various power reactances are briefly reviewed and the issues towards achieving a programmable EPI are described. In Section III, a *direct reference generation* method that is critical in accomplishing the goal of a programmable EPI is presented. In Section IV, several critical design considerations regarding the hardware design, the control and their effects on the actual EPI performance are explained. Finally, a dynamically programmable and re-configurable (multi-functional) EPI is used to demonstrate the general principle of this systematic approach in Section V.

II. Review of Existing Emulated Power Reactances

A. *Types of Emulated Power Reactances*

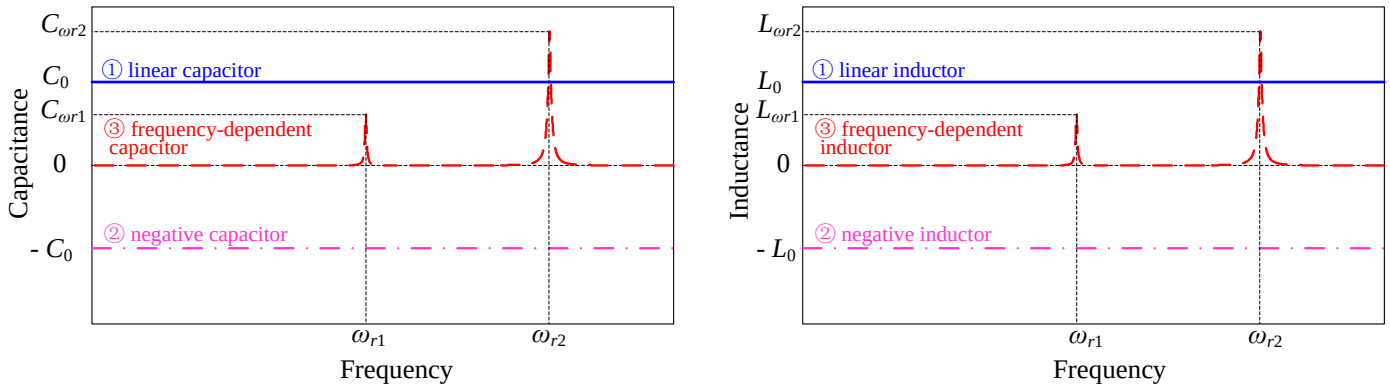

(a) (b)

Fig. 2. Illustration of (a) a linear capacitor, a negative capacitor, a frequency-dependent capacitor and (b) a linear inductor, a negative inductor, a frequency-dependent inductor in the frequency domain.

If emulated resistance is not considered, programmable reactance can be classified into three categories:

(i) *Linear inductor/capacitor*. A linear inductor/capacitor has a positive and frequency-independent inductance/capacitance value (represented as curve ① in Fig. 2). Physical inductors/capacitors belong to this category. An emulated linear inductor/capacitor is useful for replacing its physical counterparts in applications where size, weight and sometimes reliability are of major concern. Both DC and AC versions of emulated linear inductor/capacitor have been reported [4], [7], [8], [12], [13].

(ii) *Negative inductor/capacitor*. Like a linear inductor/ capacitor, a negative inductor/capacitor also has a frequency independent inductance/capacitance profile except that its value is negative (represented as curve ② in Fig. 2). These types of impedance do not exist physically. Previously, a negative inductor has been emulated [14] but no similar work has been reported for the negative capacitor. Applications of a negative inductor include the cancellation of the voltage drop attributed to line inductance along the transmission line.

(iii) *Frequency-dependent inductor/capacitor*. As illustrated in curve ③ in Fig. 2, typical frequency-dependent inductor/capacitor usually has inductance/capacitance values around some selective band-pass frequencies (such as ω_{r1}, ω_{r2}). This type of EPI can be used in the forms of an SVC, an active filter and many other types of FACTS devices through which compensating power at selective frequencies (e.g. the fundamental and/or its higher harmonic frequencies) are generated [9]–[11].

B. *Issues of Existing Control Methods for Achieving a Programmable Emulated Power Impedances*

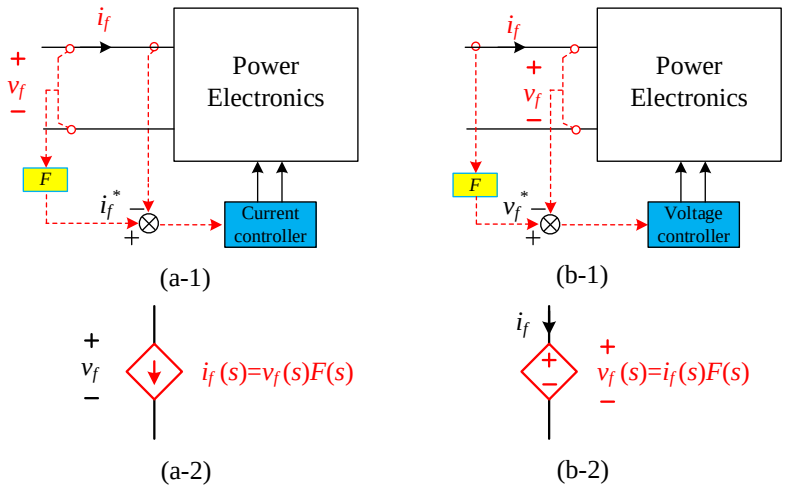

Fig. 3. Control diagram of an emulated power impedance based on (a-1) voltage-controlled current source method and (b-1) current-controlled voltage source method, together with their equivalent electrical models (a-2) and (b-2), respectively.

Fig. 3(a) and Fig.3(b) show the control block diagrams of existing EPIs under current-control and voltage control schemes, respectively. Current control involves the control of the terminal current i_f based on the measured terminal voltage v_f (Fig. 3(a)) to follow a reference signal i_f^*. Voltage control requires a voltage reference of v_f^* and the regulation of the terminal voltage v_f based on the measured i_f (Fig. 3(b)). Essentially, an EPI based on these methods becomes a (terminal) current-controlled voltage source (CCVS) (Fig. 3(a-2)) or a (terminal) voltage controlled current source (VCCS) (Fig. 3(b-2)). In both methods, the reference signals are generated through an impedance control function *F*. If the desired impedance to be emulated has an *s*-domain transfer function of Z_e(s), then *F* should satisfy

$$F(s) = 1/Z_e(s) \tag{2}$$

for VCCS method, and

$$F(s) = Z_e(s) \tag{3}$$

for CCVS method, where $F(s)$ is the *s*-domain expression of *F*. The $F(s)$ in (2) and (3) for four different types of impedances are summarized in Table I. For frequency-dependent inductor/capacitors, however, they cannot be expressed in terms of Z_e(s) due to its frequency-dependent profile. Conventionally, *F* is realized by manipulating the phasor of i_f or v_f in a rotating *dq* frame [7], [9]–[11].

Table I. Impedance Control Function *F* for emulating various power reactance

	Impedance Control Function *F*	
Control method / EPI Type	Voltage controlled current source	Current controlled voltage source
Linear capacitor (C_e)	$sC_e(s)$	$1/[sC_e(s)]$
Linear inductor (L_e)	$1/[sL_e(s)]$	$sL_e(s)$
Negative capacitor ($-C_e$)	$-sC_e(s)$	$-1/[sC_e(s)]$
Negative inductor ($-L_e$)	$-1/[sL_e(s)]$	$-sL_e(s)$
Frequency-dependent capacitor	Achieved in *dq* rotating frame	
Frequency-dependent inductor		

From Table I, the issues of existing control methods towards achieving a programmable emulated power reactance can be identified as follows:

(1) The impedance control function for many emulated power reactance contains a differentiator or an integrator. The use of a differentiator could lead to noise issues in the control circuit [6], [8], while the use of an integrator could introduce undesirable DC-offset into the reference signal which must be properly compensated [4], [7], [13], [14]. The presence of differentiator or integrator makes the practical EPI implementation cumbersome and the resulting dynamic performance poor. This explains why most existing EPI are designed with a fixed impedance value and are applied under a single operating condition.

(2) Each type of EPI requires a distinctive impedance control function for reference generation. It is therefore not straightforward to change the impedance type of an EPI. At present, no EPI that can emulate several types of impedances has been reported.

The above analysis indicate that, in order to achieve true programmability, a simple EPI control method which (i) does not involve differentiators or integrators and (ii) can be easily configured to emulate different types of EPI will be required.

III. Proposed Solution Based On Direct Reference Generation

A. *Basic Principles of Direct Reference Generation*

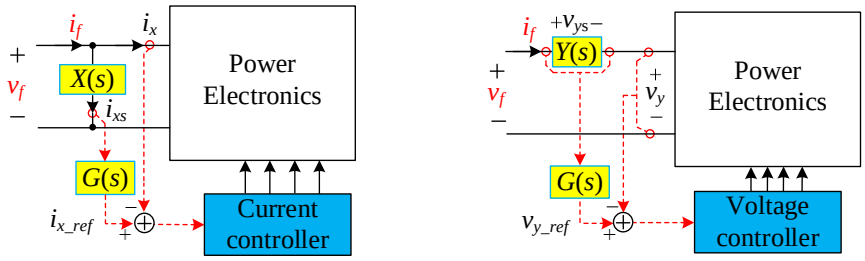

(a) (b)

Fig. 4. Direct reference generation technique for emulating a power impedance based on (a) current control current source method and (b) voltage control voltage source method.

A generalized approach to emulating a power impedance is described in this section for the current and voltage control schemes. Fig. 4(a) shows one proposed approach to controlling the EPI by direct reference generation. Different from the methods described in Fig. 3 (a), the method here does not require a

differentiator or integrator. Instead, it involves only a voltage sensing network, i.e., the parallel impedance $X(s)$ and a simple impedance control function $G(s)$ to generate the current reference signal. In particular,

$$i_{x\_ref}(s) = i_{xs}(s)G(s), \tag{4}$$

where $i_{xs}(s)$ is the current of the sensing impedance $X(s)$ and $i_{x\_ref}(s)$ is the reference of the input current of the power converter $i_x(s)$.

If a perfect current controller is assumed, i.e., $i_{x\_ref}(s) = i_x(s)$, then

$$i_f(s) = i_{xs}(s) + i_x = \left[G(s)+1\right] i_{xs}(s). \tag{5}$$

As a result, the impedance $Z_e(s)$ which the system emulates (including the effect of $X(s)$) is

$$Z_e(s) = \frac{v_f(s)}{i_f(s)} = \frac{v_f(s)}{\left[G(s)+1\right] i_{xs}(s)} = \frac{X(s)}{G(s)+1}. \tag{6}$$

In its simplest form with $G(s)=K$ (K is a positive constant), (6) becomes

$$Z_e(s) = \frac{1}{(K+1)\dfrac{1}{X(s)}}. \tag{7}$$

According to (7), the reciprocal (or the admittance) of $Z_e(s)$ is an amplified version (K+1 times amplification) of the admittance of $X(s)$. If a small capacitor C_o is used as the sensing impedance, i.e., $X(s) = 1/(sC_o)$, then the emulated impedance is simply

$$Z_e(s) = \frac{1}{(K+1)(sC_o)} = \frac{1}{s\left[(K+1)C_o\right]} = \frac{1}{sC_e}, \tag{8}$$

in which the equivalent capacitor C_e has a capacitance value of $(K+1)C_o$. In this way, a linear capacitor can be emulated without taking a differentiation or integration. By adjusting the parameter K, one is able to change the capacitance value conveniently.

Based on duality principle, another form of impedance emulation method can be derived as shown in Fig.4 (b), in which a series current sensing impedance $Y(s)$ is employed to generate the voltage reference $v_{y\_ref}(s)$. Assuming perfect voltage control, i.e., $v_{y\_ref}(s) = v_y(s)$, $Z_e(s)$ becomes

$$Z_e(s)=\frac{v_f(s)}{i_f(s)}=\left[G(s)+1\right]\frac{v_{ys}(s)}{i_f(s)}=\left[G(s)+1\right]Y(s). \tag{9}$$

If $G(s) = K$, then

$$Z_e(s)=(K+1)Y(s). \tag{10}$$

Equation (10) means that $Z_e(s)$ is a "K+1" amplified version of $Y(s)$. It implies that a small inductor L_o can be used as a sensing impedance to emulate a large linear inductor L_e with inductance value of $(K+1)L_o$. Again, no differentiation or integration is needed in this method.

Essentially, an EPI based on the above methods becomes a current-controlled current source (CCCS) in Fig. 4(a), or a voltage-controlled voltage source (VCVS) in Fig. 4(b). The proposed control strategy enables a direct generation of the reference signal without the need for phase conversion which is originally achieved through an integrator/differentiator. Thus, the delay in reference signal generation is minimal. This will significantly improve the dynamic accuracy of the impedance emulation [7].

B. *Towards A Programmable Emulated Power Impedance*

A fully programmable and re-configurable EPI should allow not only the value, but also the type of the EPI to be changed. According to (6) and (9), the type of EPI can be controlled by changing $G(s)$. For (6), if $X(s)=1/(sC_o)$, and

(i) $G(s) = k_p$, then $Z_e(s) = 1/[s(k_p+1)C_o]$;

(ii) $G(s) = -k_p$ then $Z_e(s) = 1/[s(1-k_p)C_o]$;

(iii) $G(s)=\dfrac{k_r\omega_c s}{s^2+\omega_c s+\omega_r{}^2}$, then $Z_e(s)=\dfrac{1}{sC_o\left[\dfrac{s^2+(k_r+1)\omega_c s+\omega_r{}^2}{s^2+\omega_c s+\omega_r{}^2}\right]}$;

(iv) $G(s)=\dfrac{-k_r\omega_c s}{s^2+\omega_c s+\omega_r{}^2}$, , then $Z_e(s)=\dfrac{1}{sC_o\left[\dfrac{s^2+(1-k_r)\omega_c s+\omega_r{}^2}{s^2+\omega_c s+\omega_r{}^2}\right]}$.

In these four cases, $G(s)$ is a proportional (P) function, a negative proportional function ($-P$), a 2nd order resonant (R) function, and a negative 2nd order resonant ($-R$) function, respectively. It can be concluded that:

(i) If G(s) is a P function, then $Z_e(s)$ is a *linear capacitor* with capacitance value of $(k_p+1)C_o$, as given previously in (8);

(ii) If G(s) is a $-P$ function, then $Z_e(s)$ is a *negative capacitor* with capacitance value of $(1-k_p)C_o$ (assume that $k_p \geq 1$). If $k_p \gg 1$, then the negative capacitor here possesses almost has the same impedance magnitude as the linear capacitor in (i) except that the phase is shifted by 180°.

(iii) If G(s) is an R function, then $Z_e(s)$ is a *quasi-frequency-dependent capacitor* because it has a capacitance of $(k_r+1)C_o$ at frequency ω_r since

$$Z_e(s)\big|_{s=j\omega_r} = \frac{1}{j\omega_r C_o(k_r+1)}, \tag{11}$$

and a capacitance of C_o at low frequencies (when $s \ll 1$) or at high frequencies ($s\to\infty$), $Z_e(s)$ since

$$Z_e(s)\big|_{s\ll 1} = Z_e(s)\big|_{s\to\infty} = \frac{1}{sC_o}. \tag{12}$$

If C_o is sufficiently small such that $Z_e(s)$ is almost like an open circuit at the low frequency range and the passing band of the R function defined by ω_c is narrow, then the quasi-frequency-dependent capacitor can be used to approximate an ideal frequency-dependent capacitor.

(iv) If G(s) is an $-R$ function, then $Z_e(s)$ is a *quasi-frequency-dependent inductor* with an effective inductance of $1/(\omega_r^2 C_o(k_r-1))$ at frequency ω_r. At low frequencies (when $s \ll 1$) or at high frequencies ($s\to\infty$), $Z_e(s)$ is equivalent to a capacitor with a capacitance value of C_o. Analogous to (iii), a quasi-frequency-dependent inductor can be used to approximate an ideal frequency-dependent inductor provided that C_o is sufficiently small and the passing band of the $-R$ function is narrow.

The frequency responses of Z_e (in the form of admittance) based on C_o = 10 μF, k_p = 100, k_r = 100, ω_r = 628 rad/sec and ω_c = 0.628 when $G(s)$ is configured as a P, $-P$, R and $-R$ function are calculated and shown in Fig. 5. Clearly, with a P and $-P$ impedance control function, $Z_e(s)$ is emulating a linear capacitor of 1010 μF and a negative capacitor of -990 μF, respectively. When $G(s)$ is an R function, $Z_e(s)$ is a quasi-frequency-dependent capacitor since the frequency responses of Z_e(s) overlaps with the C_o = 10 μF admittance line for all frequencies except at ω_r = 628 rad/sec when it intersects with the 1010 μF admittance

line. Finally, when $G(s)$ is an $-R$ function, $Z_e(s)$ is a quasi-frequency-dependent inductor with an inductance of 2.56 mH at ω_r = 628 rad/sec and a capacitance of C_o = 10 μF at other frequencies. The frequency-dependent impedance profile together with its almost zero admittance of at the low frequency ranges (and thus nearly null responses at these frequencies) offers the feasibility of using a quasi-frequency-dependent capacitor/inductor to approximate an ideal frequency-dependent capacitor/inductor.

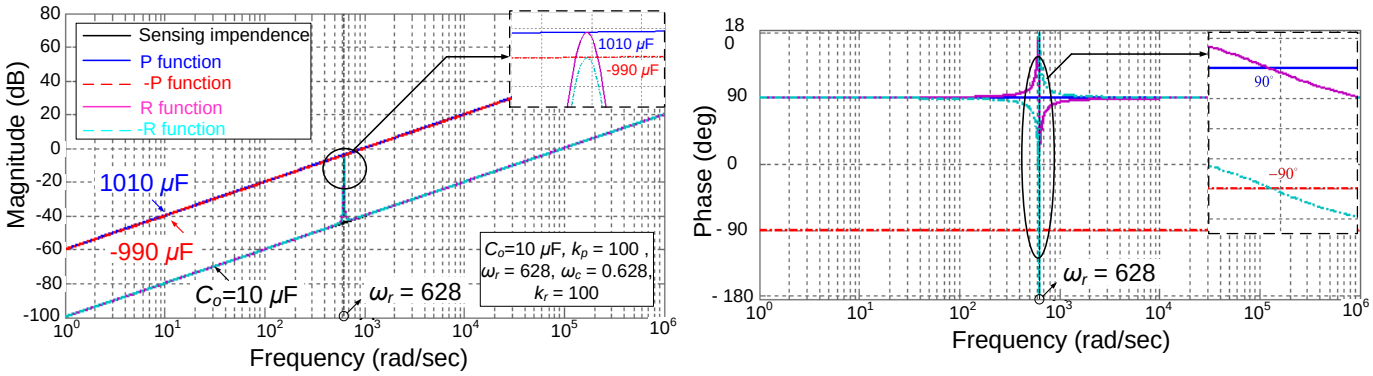

Fig. 5. Frequency responses of the emulated power impedance $Z_e(s)$ (in the form of admittance) given the impedance control function $G(s)$ configured as a P function, a $-P$ function, a 2nd order R function (with a pair of resonant poles at ω_r), and a 2nd order $-R$ function (with a pair of resonant poles at ω_r).

By configuring $G(s)$ as a P, $-P$, R or $-R$ function, the EPI can be flexibly changed between a *linear capacitor*, a *negative capacitor*, a *quasi-frequency-dependent capacitor* or a *quasi-frequency-dependent inductor* based on CCCS method (see Fig. 6). Note that $G(s)$ can also be configured to emulate a linear inductor and a negative inductor. This will require $G(s)$, however, to incorporate two integrators which are undesirable. Alternatively, if the VCVS method shown in Fig. 4(b) is employed, then based on (9) and assuming $Y(s)=sL_o$, $Z_e(s)$ can be easily configured as a *linear inductor*, a *negative inductor*, a *quasi-frequency-dependent inductor* or a *quasi-frequency-dependent capacitor* by configuring $G(s)$ as a P, $-P$, R or $-R$ function, respectively (Fig. 6).

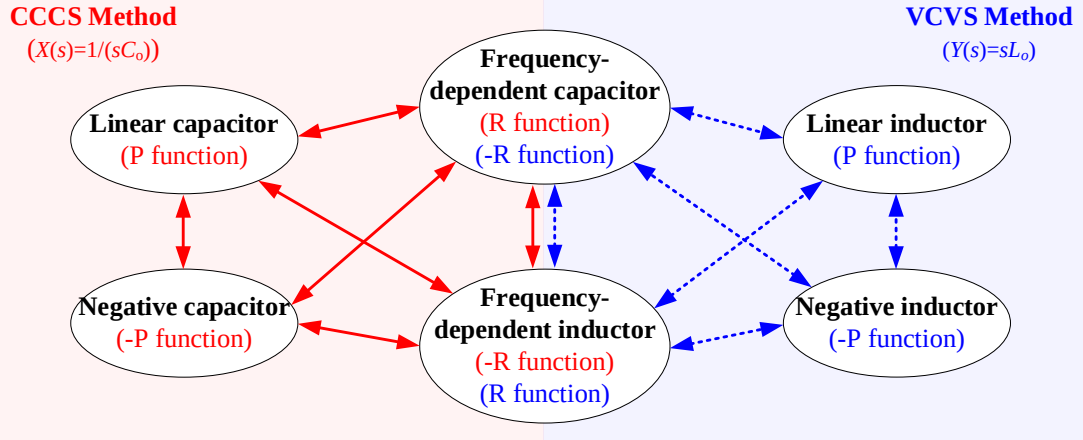

Fig. 6. Transitional diagram among various emulated power impedances.

It should be noted that each emulation method given in Fig. 4 can emulate four types of EPI. If all the six types of EPI are needed, a combined system augmented with both series and parallel sensing impedances can be employed (as shown in Fig. 7). A complete emulation of the six types of EPI can be achieved by switching between the CCCS and VCVS mode of operation.

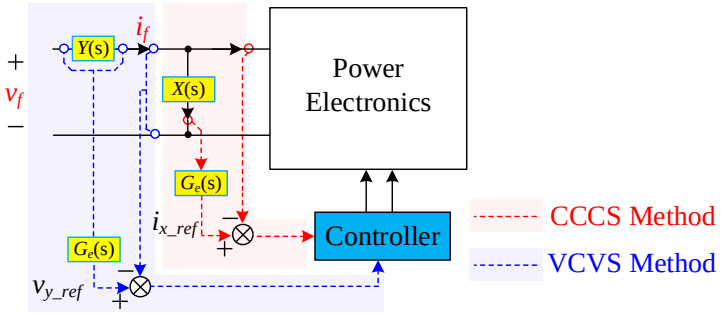

Fig. 7. A combined CCCS-VCVS method which incorporates a parallel sensing and a series sensing impedance $X(s)$ and $Y(s)$.

C. *Further Extensions of Programmability and Re-configurability*

$G(s)$ may be further configured as a combination of the four functions (P, $-P$, R and $-R$), e.g., $P+R$, $P-R$, $-P+R$, $-P+R$, etc. For instance, if $G(s)=k_p+\frac{k_{r1}\omega_c s}{s^2+\omega_c s+\omega_{r1}^{\ 2}}+\frac{k_{r2}\omega_c s}{s^2+\omega_c s+\omega_{r2}^{\ 2}}$, which contains one P function and two R functions, then based on CCCS method and assuming $X(s)=1/(sC_o)$, the frequency response of $Z_e(s)$ can be illustrated as shown in Fig. 8.

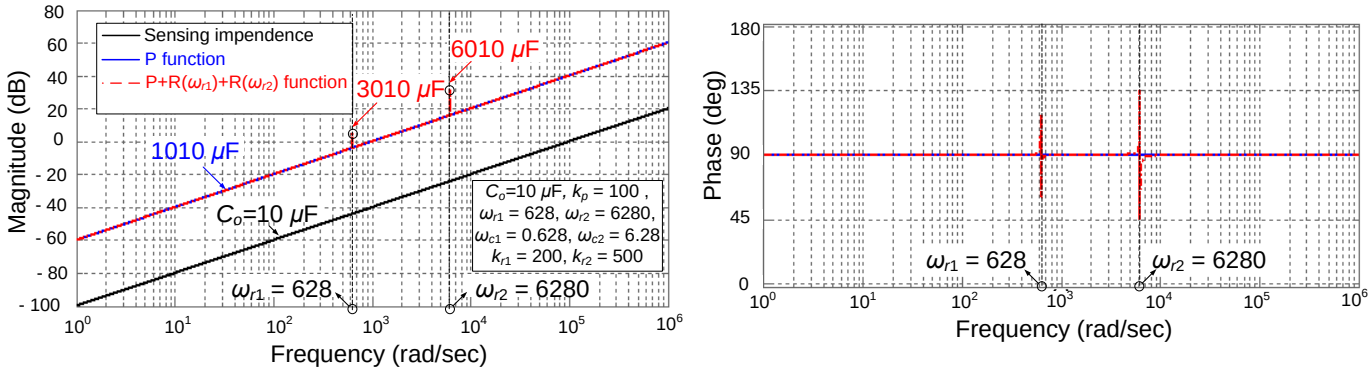

Fig. 8. Frequency responses of the emulated power impedance $Z_e(s)$ (in the form of admittance) when the impedance control function $G(s)$ contains one P term and two 2nd order R terms (with two pairs of resonant poles at ω_{r1} = 628 and ω_{r2} = 6280).

Due to the P term in $G(s)$, $Z_e(s)$ behaves like a linear capacitor with a capacitance value of $(k_p+1)C_o$ (i.e., 1010 μF) for all frequencies. The two R terms, on the other hand, provide an additional capacitance gain at the frequencies of ω_{r1} and ω_{r2}. The equivalent capacitance is therefore increased to $(k_p+k_{r1}+1)C_o$ (i.e., 3010 μF) at ω_{r1}, and $(k_p+k_{r2}+1)C_o$ at ω_{r2} (i.e., 6010 μF). Such an EPI is also a frequency-dependent capacitor. The inclusion of multiple R functions may be useful for filtering out high order harmonics in power system applications such as an active filter.

IV. Design Considerations

A. *Hardware Design Considerations*

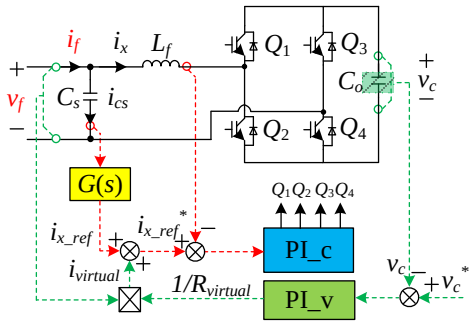

(a-1)

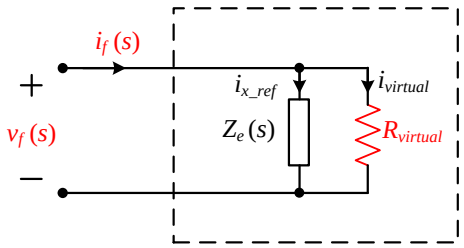

(a-2)

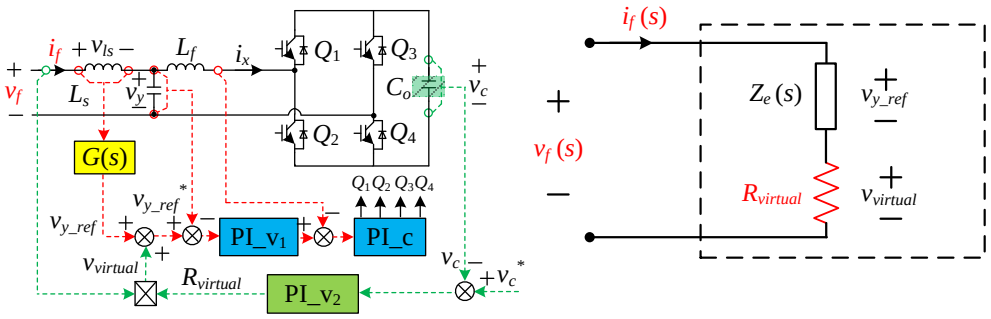

(b-1) (b-2)

Fig. 9. Practical hardware and control implementation of an emualted power reactance based on (a-1) CCCS and (b-1) VCVS method. Their electrical equivalents are shown in (a-2) and (b-2).

Fig. 9 (a-1) and (b-1) illustrate how to use a full-bridge converter to set up an EPI based on the proposed CCCS and VCVS method, respectively. To provide the energy storage required, a capacitor C_o is connected to the DC-link of the full-bridge converter. Like any typical power electronic converter designs, the cost, the size and the efficiency of the system must be optimized. In the case of designing an EPI, there are two additional considerations:

(i) The energy storage capability of C_o should match the actual application requirement INSTEAD of the energy storage capability of the EPI which the system is emulating.

In most AC applications, the energy storage capability of C_o should be the same as that of the power reactance which the system is emulating. For instance, if an AC capacitor with a capacitance of C_{AC} is emulated which is applied in shunt with an AC grid, then C_o should be designed such that

$$C_{AC}V_{f\_peak}^{\ 2} = C_oV_c^{\ 2} \tag{13}$$

where V_{f_peak} is the peak terminal voltage of C_{AC} which is equal to the AC voltage amplitude, and V_c is the DC-link voltage of the full-bridge converter.

In DC applications, however, the required energy storage in C_o can be much smaller. This is because a DC power reactance typically stores a large portion of redundant energy. One example is the DC-link capacitor $C_{dc\text{-}link}$ widely employed in single-phase PFC applications for reducing the double-line frequency voltage ripples [15]. It can be calculated that, with a 1% voltage ripple on the DC-link of the PFC, only 1.99% of the total energy stored in the $C_{dc\text{-}link}$ is useful for compensating

the double-line frequency voltage variations, while the rest of stored energy is redundant [16]. In such applications, if an EPI is used to emulate and replace the DC-link capacitor $C_{dc\text{-}link}$, the minimum C_o should satisfy

$$\eta_E C_{dc-link} {V_{f\_peak}}^2 = C_o V_c^2, \quad (0 < \eta_E < 1) \tag{14}$$

where η_E is energy utilization rate (which is the ratio of the useful energy to the total energy stored in $C_{dc\text{-}link}$), V_{f_peak} is the peak DC-link voltage applied to $C_{dc\text{-}link}$. Some design examples for selecting C_o in PFC applications can be found in [15], [16].

(ii) The sensing impedance should have negligible effect on the proper operation of the system.

The incorporation of a sensing impedance, such as C_s or L_s, increases the order of the full-bridge converter. For applications in the low frequency range (e.g. from DC up to several hundred Herz), if C_s or L_s are sufficiently small, its effect on the overall system will be negligible. As a result, the system can still be controlled as a conventional *L* type full-bridge converter in the case of Fig. 9(a) and a *LC* type full-bridge converter in the case of Fig. 9(b).

B. *Control Strategies*

The detailed control block diagrams are shown in Fig. 9(a-1) and (b-1) for the proposed CCCS and VCVS control methods, respectively. Compared with Fig. 4, an additional voltage control loop for regulating v_c is included to compensate the power losses of the system.

For the CCCS (Fig. 9(a-1)), the regulation of v_c is realized by modifying the ideal EPI (i.e., Z_e(s) in Fig. 1) into an $R_{virtual}$-Z_e parallel impedance network shown in Fig. 9(a-2). Here, $R_{virtual}$ is a virtual resistor representing the overall system losses. To achieve this, the terminal voltage v_f is firstly sensed and divided by $R_{virtual}$ to generate the current $i_{virtual}$ through it. This current is then added to i_{x_ref} to form the new reference ${i_{x\_ref}}^*$ for the converter to track. To properly compensate the power losses, the value of $R_{virtual}$ is dynamically predicted through a *PI* controller which regulates the average v_c at the target value v_c^*. This is possible because the absorbed energy and hence the voltage v_c varies according to the change of $R_{virtual}$. Similarly, for

the VSVC method given in Fig. 9(b-2), the regulation of v_c is achieved by mimicking an $R_{virtual}$-Z_e series impedance network that is achieved by sensing the terminal current i_f to derive $v_{virtual}$, which is added to v_{y_ref} to obtain the new reference $v_{y\_ref}{}^*$.

The inner-loop current controller for CCCS and the voltage controller for VCVS are conventional controllers used for an *L* type and an *LC* type full-bridge converters. In this work, a simple *PI* controller is used as the current controller for CCCS, and a dual-loop controller is used as the voltage controller for VCVS.

C. *Bandwidth of Emulated Power Impedance*

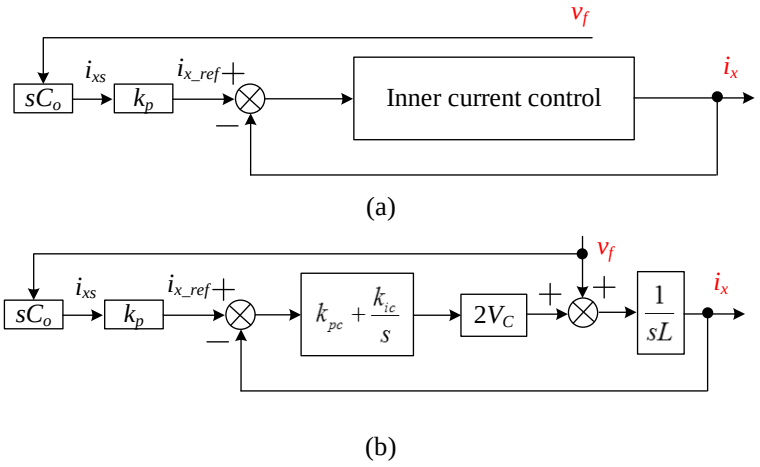

Fig. 10. Simplified closed-loop small-signal system model of Fig. 10 (a-1) for emulating a linear capacitor of $C_e = (k_p+1)C_o$.

The frequency response of an EPI can be derived by performing a closed-loop small-signal analysis over the entire system. For instance, a CCCS system can be generally modeled as shown in Fig. 10(a), where the bus voltage v_c is assumed constant (i.e., $v_c = V_c$). It can be seen that the dominating factor that limits the bandwidth of the EPI is that of the inner current loop: the higher the bandwidth of the inner current loop, the higher the EPI's bandwidth. Therefore, an optimal design of the inner current loop is necessary if high bandwidth is needed. Similarly, the limiting factor of the EPI bandwidth for a VCVS system is that of the inner voltage loop. An emulated linear capacitor based on Fig. 9(a-1) (where $G(s)$ is set to k_p) is examined here for discussing the factors that will affect the operating bandwidth of the EPI. The simplified model is shown in Fig. 10 (b). Solution of the model in Fig. 10 gives the closed-loop emulated impedance $Z_e(s)$ as

$$Z_e(s)=\frac{v_f(s)}{i_f(s)}=\frac{v_f(s)}{i_x(s)+i_{xs}(s)}=\frac{s^2L_f+s\left(2k_{pc}V_c\right)+2k_{ic}V_c}{s^3C_oL_f+s^2\left(2C_oV_ck_{pc}\right)\left(1+k_p\right)+s\left[1+2C_o\left(1+k_p\right)k_{ic}V_c\right]}, \quad (15)$$

where k_{pc} and k_{ic} are the proportional and integral gain of the *PI* current controller, respectively.

At low frequencies when $s \ll 1$,

$$Z_e(s)\big|_{s\to 0} \approx \frac{1}{s\left[C_o\left(k_p+1\right)+\dfrac{1}{2k_{ic}V_c}\right]} \approx \frac{1}{sC_o\left(k_p+1\right)}, \quad \left(k_{ic}V_c \gg 1\right) \quad (16)$$

and at high frequencies,

$$Z_e(s)\big|_{s\to\infty}=\frac{1}{sC_o} \quad (17)$$

Equations (16) and (17) indicate that the EPI is an amplified version of C_o at low frequencies and reverts to C_o at high frequencies. Fig. 11 shows the frequency response plots (in the form of admittance) of the EPI calculated based on (15). It can be observed that the EPI under test behaves like a linear capacitor of $C_e = (k_p+1)C_o = 1010\ \mu$F only at low frequencies (up to around 2,000 rad/sec). Clearly from Fig. 10 (b), one can see that the bandwidth of the inner current loop is determined by (i) the PI compensator (ii) the DC-link voltage V_c, and (iii) the output filter inductor L_f. A larger L_f tends to decrease the loop gain of the current loop. However, a larger V_c and/or an optimized compensator (including advanced nonlinear controller) design can make up for the decrease of the loop gain, resulting a similar or even extended EPI bandwidth (assuming that the system is still stable). If the power rating of the system is very large such that a huge L_f is unavoidable, then one can either increase the switching frequency and/or adopt a different circuit topology, for instance, from two-level to multi-level, to reduce the filtering inductance. The output capacitor C_o, on the other hand, has nothing to do with the bandwidth of the EPI because it is not involved in the inner current loop. Instead, C_o will only offset the frequency response curve of the EPI vertically, which can be concluded from (15).

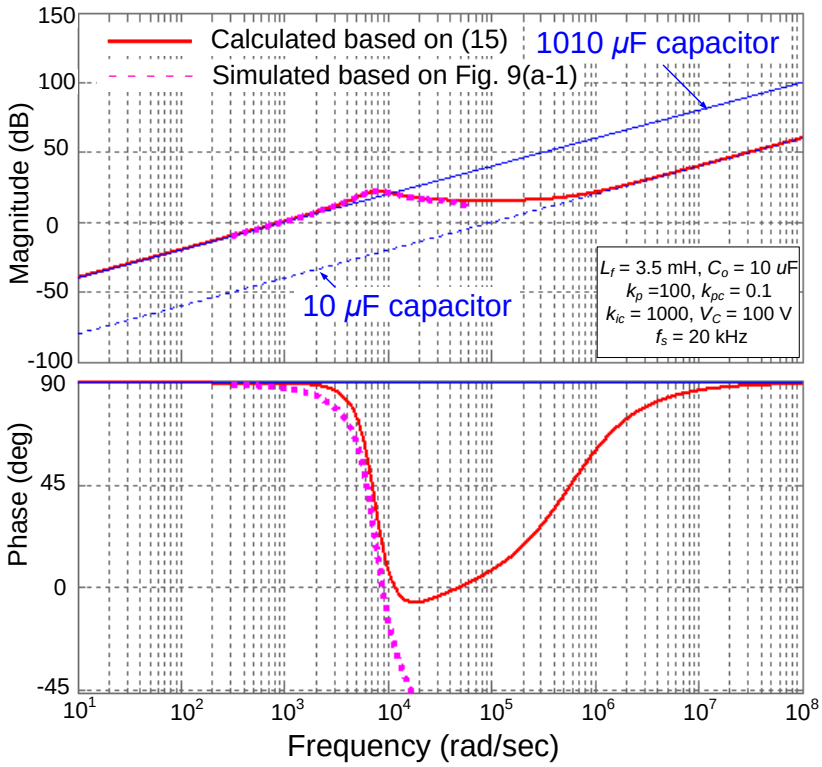

Fig. 11. The frequency response plots (in the form of admittance) of an EPI of 1010 μF capacitance value with a PI current controller (calculated based on (15)) and a PI current controller (through simulation based on the setup of Fig. 9(a-1)).

In practice, the delays due to the sampling of the analogue-to-digital converter (ADC) and the computational process of the digital controller can further reduce the bandwidth of the EPI. However, their effect to the bandwidth of the EPI is generally insignificant at low-frequency ranges. The simulated frequency response of the EPI that incorporates the effect of the computational and the sampling delay is shown in Fig. 11. It can be observed that the simulation model has been predicted accurately by the simplified model of (15) up to around 9,000 rad/sec, beyond which the delays gradually takes over frequency response. The sampling theorem predicts that the bandwidth an EPI cannot exceed the Nyquist frequency. Therefore, an EPI may not be suitable for applications that involve very-high-bandwidth operation.

V. Experimental Verification

A. *Steady-State Performance of a Programmable Power Impedance Based on Direct Reference Generation*

Table II. Design Specifications for Testing Various Emulated Power Reactance

Design Parameter	Value	Design Parameter	Value
Average voltage for R_o	48 V	Sensing capacitor C_s	10 μF
Switching frequency f_s	25 kHz	Sensing inductor L_s	1 mH
Load R_o	100 Ω	DC-link capacitor C_o	470 μF/ 350 V
Filter inductor L_f	3.5 mH	Switches Q_1– Q_4	IRG4PC30FDPbF

To evaluate the performance of an EPI based on the proposed direct reference generation method, four different experiments have been conducted. The experiments include the emulation of a linear capacitor, a linear inductor, a frequency-dependent capacitor and a frequency-dependent inductor. The purpose of the first two experiments is to check the steady-state performance of the CCCS and VCVS method, respectively. The last two experiments are to verify the feasibility of achieving a fully programmable power impedance profile through the re-configuration of the impedance control function $G(s)$. The hardware configuration of the EPI is the same as that shown in Fig. 9. The control of the converter is implemented using a DSP (Model: TMS320F28069). The detailed circuit parameters and component specifications are listed in Table II.

1) Emulation of a DC Linear Capacitor

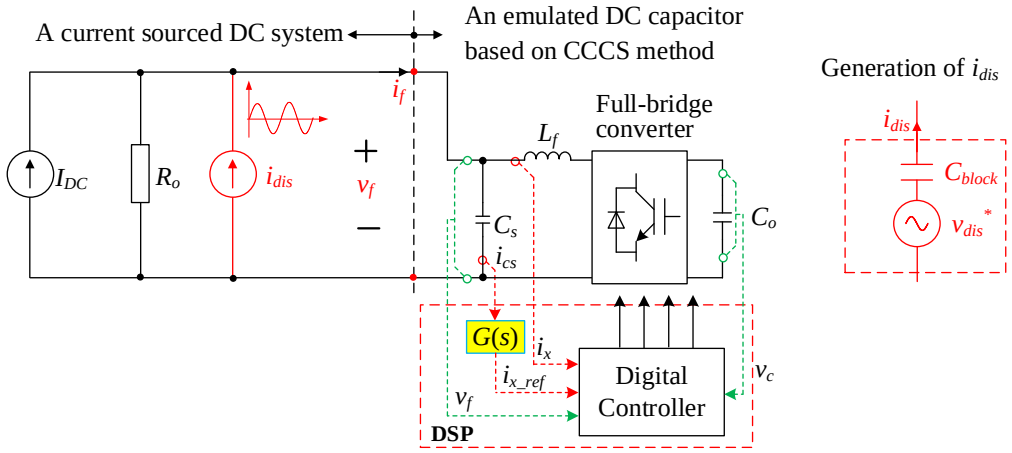

Fig. 12. (a) Experiment setup for testing the V–I responses of an emulated linear capacitor and a physical capacitor and (b) schematic diagram of i_{dis} generation.

Fig. 12(a) shows the setup for the first experiment. A DC system comprising a DC current source I_{DC}, a disturbing current source i_{dis} and a resistive load R_o are used to test the performance of an emulated DC linear capacitor. Here, I_{DC} is manually tuned such that the average voltage of the load R_o is 48 V. i_{dis} is

generated by a variable frequency AC voltage source v_{dis}^* (Model: GW Instek APS-9501, output frequency range 45 Hz to 500 Hz) via a 100 μF DC voltage blocking capacitor C_{block} (Fig. 12(b)). The frequency and amplitude of i_{dis} is set at 50 Hz and 0.7 A (or 0.5 Arms), respectively. The sensing capacitor C_o is chosen as 10 μF and G(s) is set as 100. According to (8), the EPI system should be emulating a linear 1010 μF capacitor.

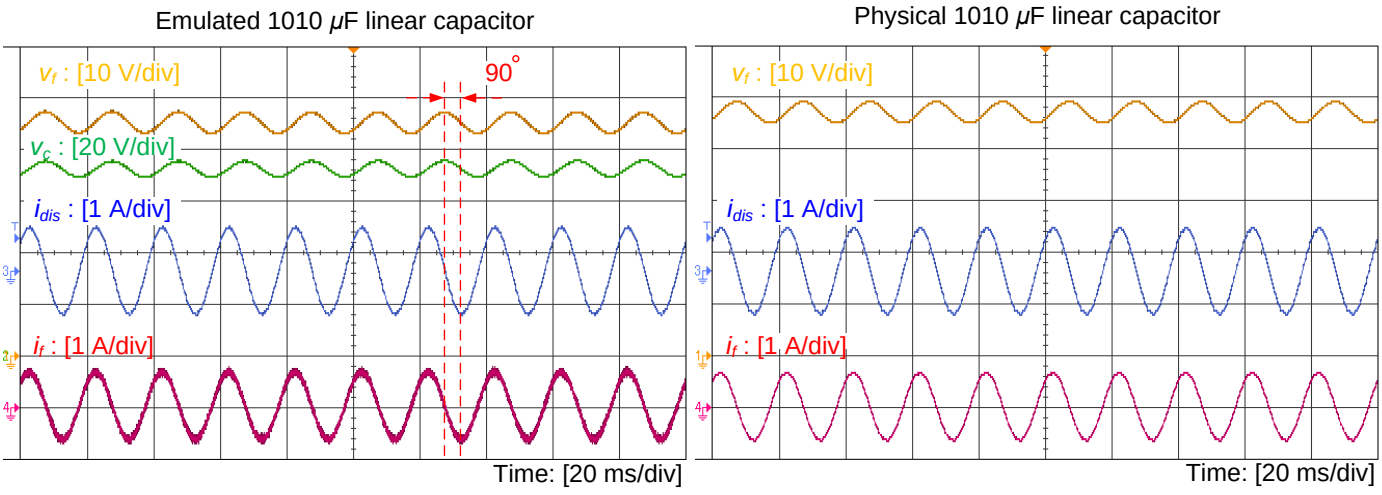

(a) (b)

Fig. 13. Measured terminal waveforms of an emulated and a real linear capacitor of 1010 μF under 50 Hz current disturbances.

The measured steady-state waveforms of v_f, i_f and v_c are shown in Fig. 13(a). It can be observed that the waveforms of both i_f and v_f are purely sinusoidal. Additionally, i_f is leading the AC portion of v_f by 90°. This indicates that the EPI is operating as a capacitor. For comparison, a real capacitor of 1010 μF is applied in the place of the emulated capacitor. The measured waveforms of i_f and v_f are shown in Fig. 13(b). Both v_f and i_f are almost identical for the emulated and the real capacitor. This confirms the accuracy of the emulated 1010 μF capacitor with the CCCS method at 50 Hz. Note, however, that the average voltage of v_f of the emulated capacitor is slightly lower (around 1 V) than that of the real capacitor. This is because a small portion of i_f, i.e., the DC offset current of $v_f/R_{virtual}$, is used for compensating converter power loss, and the average current through the load R_o is reduced.

A complete frequency responses of the emulated 1010 μF linear capacitor at other frequencies (ranging from 50 Hz to 500 Hz) are also measured and plotted in Fig. 16(a) which shall be discussed in Section V-A3).

2) Emulation of a DC Linear Inductor

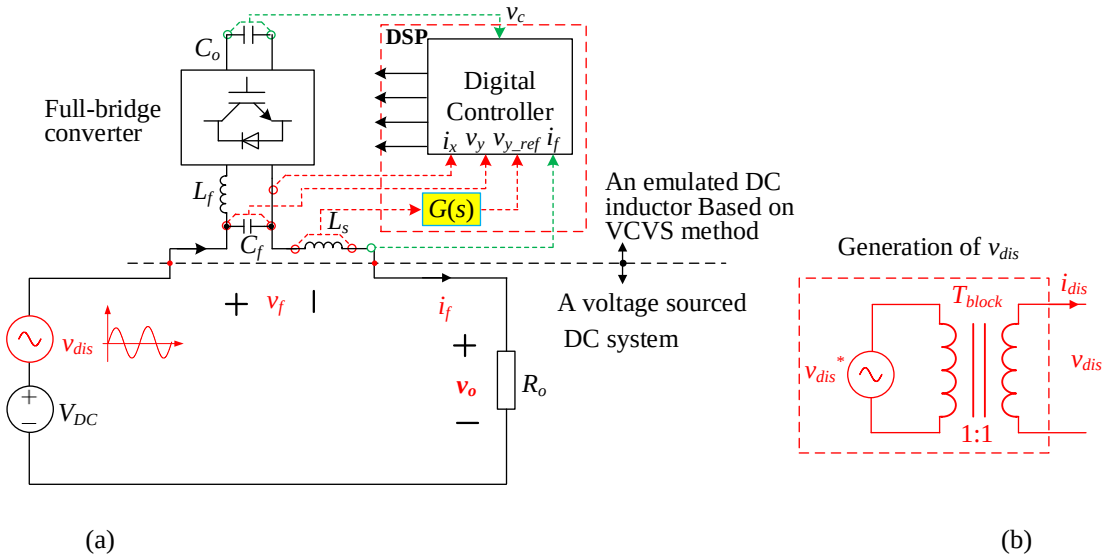

Fig. 14. Experiment setup for testing the V–I responses of an emulated linear inductor and a physical inductor and (b) schematic diagram of v_{dis} generation.

Fig. 14(a) shows the setup for testing an emulated DC linear inductor based on the VCVS method. The DC system consists of a constant DC voltage source V_{DC}, a disturbing voltage source v_{dis} (20 Vrms/50 Hz) and a resistive load R_o. Here, V_{DC} is manually set at 48 V, and v_{dis} is generated by v_{dis}^* through a 1:1 turns ratio isolation transformer for DC current bypassing (Fig. 14(b)). Since L_o = 1 mH and G(s) = 100, the EPI is equivalent to a linear inductor of 0.101 H.

Fig. 15(a) illustrates the measured waveforms of v_f, i_f and v_c of the emulated 0.101 H inductor. Again, pure sinusoidal waveforms are obtained and inductive operation is confirmed (since the AC portion of i_f is now lagging v_f by 90°). A second experiment is conducted by connecting a real 0.101 H inductor in the place of the emulated inductor, of which the waveforms of v_f and i_f are shown in Fig. 15(b). It is clear that the V-I characteristics of a physical 0.101 H inductor have been successfully emulated by the EPI based on the VCVS method.

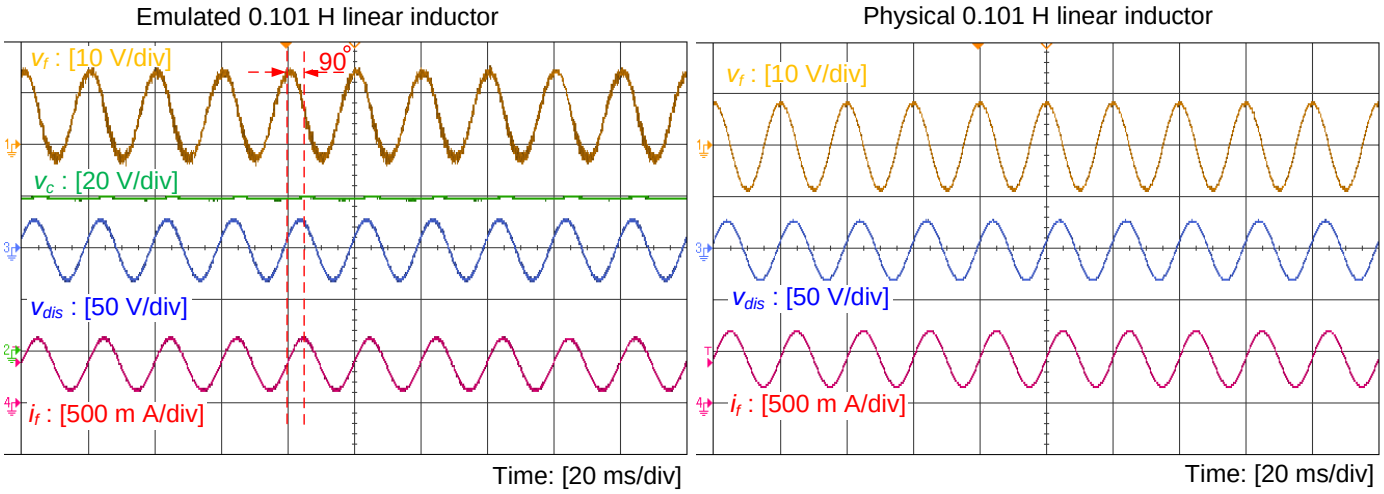

(a) (b)

Fig. 15. Measured terminal waveforms of an emulated and a real linear inductor of 0.101 H under 50 Hz voltage disturbances.

3) Emulation of a Frequency-Dependent DC Capacitor and a Frequency-Dependent DC Inductor

The hardware setup for the third and fourth experiments are identical to those illustrated in Fig. 12 and Fig. 14. The difference is that $G(s)$ is programmed as a P+R function, of which $G(s)= 20+\frac{80\times(2\times\pi\times10)s}{s^2+(2\times\pi\times10)s+(2\times\pi\times100)^2}$. Thus, the EPI should be emulating a 1010 μF capacitor and a 0.101 H inductor (101 times amplification of the sensing impedance) at 100 Hz, respectively for the setup of Fig. 12 and Fig. 14. At other frequencies, the system should emulate a 210 μF capacitor and a 0.021 H inductor (21 times of amplification of the sensing impedance), respectively.

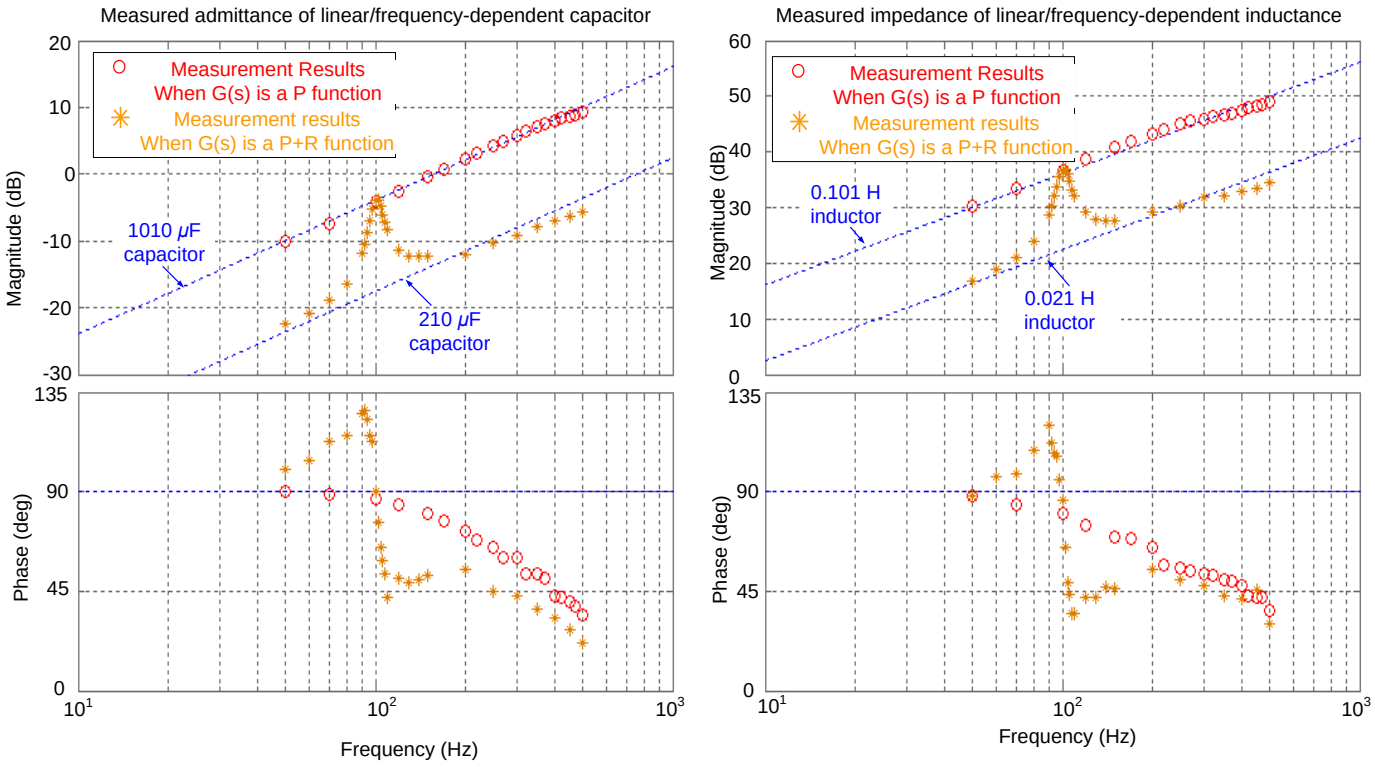

(a) (b)

Fig. 16. Measured frequency responses of (a) a linear capacitor and a frequency-dependent capacitor and (b) a linear inductor and a frequency-dependent inductor.

The measured frequency response of a linear/frequency dependent capacitor (in the form of admittance) and a linear/frequency dependent inductor (in the form of impedance) are shown in Fig. 16(a) and (b), respectively. Fig. 16(a) shows that the admittance of the emulated linear capacitor fits well with that of a 1010 μF capacitor within the frequency range of 50 Hz to 500 Hz. This confirms that the utilization of a *P* function for *G*(*s*) achieves the emulation of a linear capacitor for a wide frequency ranges. When an *P*+*R* type function is employed, the resultant admittance profile is changed in such a way that (i) it intersects with the 1010 μF admittance line only at 100 Hz and (ii) it overlaps with the 210 μF admittance line at other frequencies. These results confirm the feasibility of changing an emulated linear capacitor to an emulated frequency-dependent capacitor by incorporating an *R* function into *G*(*s*).

Similar conclusions can be made from Fig. 16(b). It can be seen that the frequency response of an emulated linear inductor is almost identical to that of an ideal 0.101 H inductor when a *P* function is

employed. As $G(s)$ is changed into a $P+R$ function, a frequency-dependent inductor that mimics a 0.101 H inductor at 100 Hz, and a 0.021 H inductor at other frequencies has been achieved.

B. *Dynamic Performance of a Programmable Power Impedance as a Multi-Functional Equipment*

In the previous session, only the steady-state performance of the EPI are examined. In many applications, both the value and the type of an EPI needs to be varied continuously or even abruptly. In this session, the dynamic performance of an EPI are reported with the proposed direct reference generation method.

1) EPI as a Dynamic DC Linear Capacitor (Changing G(s) From a P Function to Another P Function)

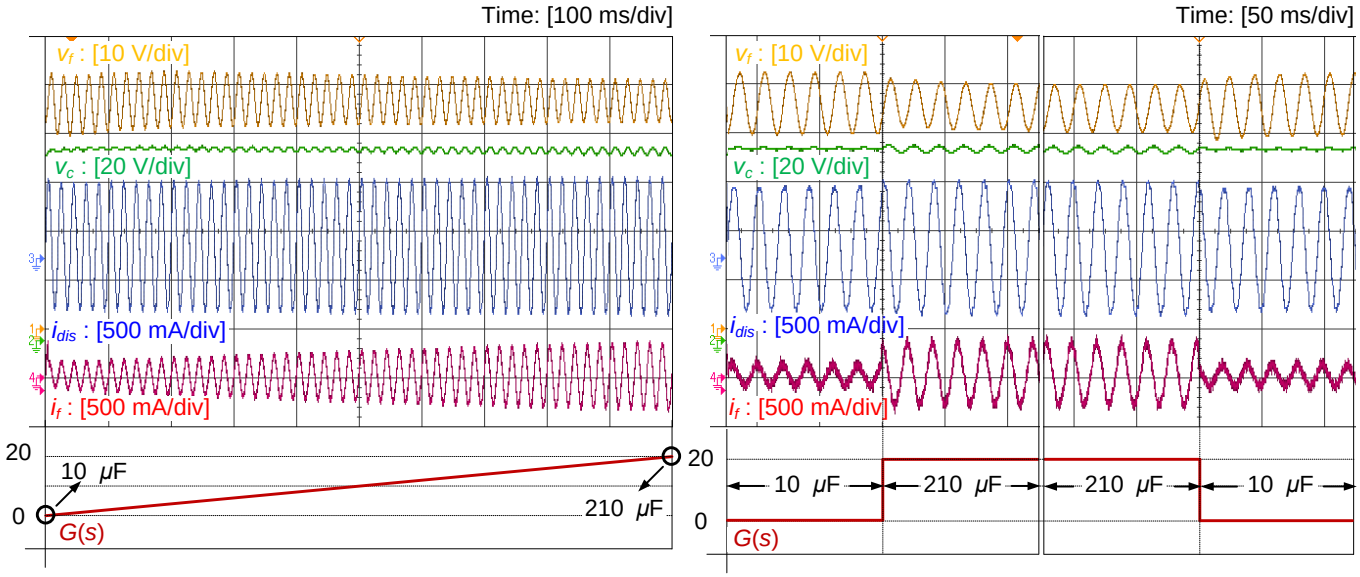

(a) (b)

Fig. 17. Performance of the EPI as a dynamic DC linear capacitor whose capacitance value is (a) smoothly changed and (b) stepped changed between 10 μF and 210 μF.

A dynamic linear capacitor is a linear capacitor with a variable capacitance value [8]. In this experiment, a dynamic DC linear capacitor is emulated by changing $G(s)$ between 0 and 20 based on the system setup shown in Fig. 12. The result will be a dynamically changing of the emulated capacitance value between 10 μF and 210 μF. Both ramp change and step change of $G(s)$ are performed and the dynamic waveforms of v_f, i_f and v_c are shown in Fig. 17(a) and (b), respectively.

From Fig. 17(a), it can be observed that the amplitude of v_f reduces and that of i_f increases with the increase of $G(s)$. This is because the emulated capacitance increase with $G(s)$, and a larger capacitance naturally provides a better filtering function for the disturbing current i_{dis}. For the same reason, the reactive power absorbed by the emulated linear capacitor also increases with G(s), leading to an increasing amplitude of v_c. In Fig. 17(b), $G(s)$ is step changed from 20 to 0 and then back to 20. The emulated capacitance is changed almost instantly with the change of $G(s)$. This can be observed by inspecting the waveforms of v_f, i_f or v_c. The amplitudes of these waveforms are instantly changed with the change of $G(s)$.

2) EPI as a Plug-and-Play Ripple Mitigator (Changing G(s) From R Function to P Function)

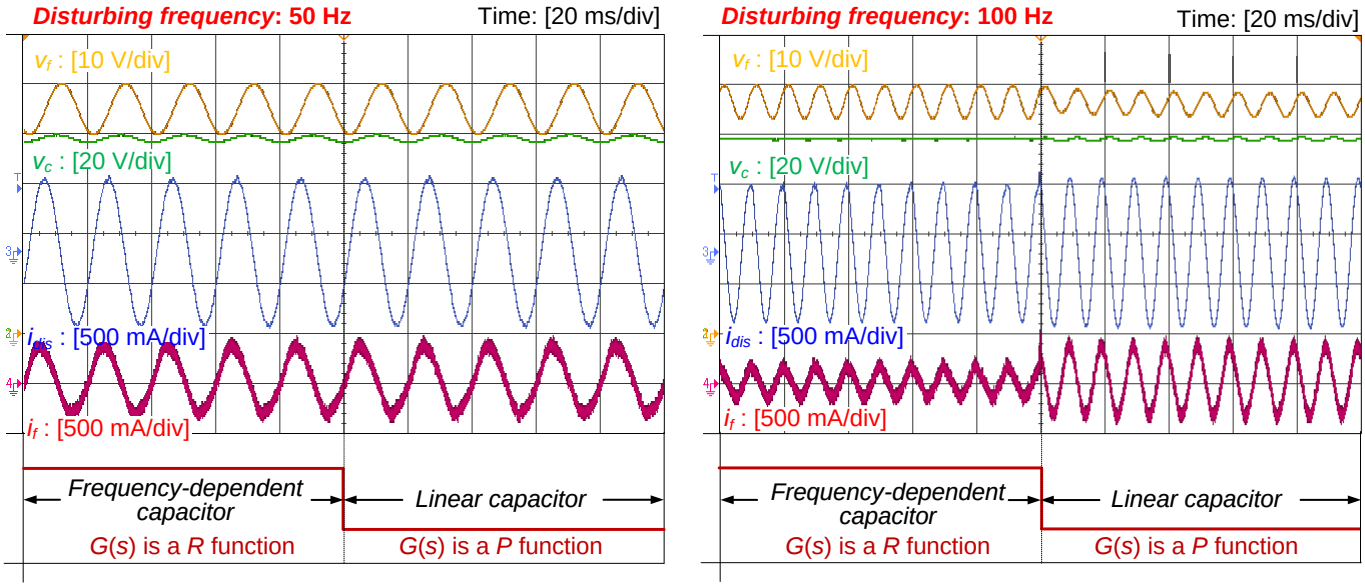

(a) (b)

Fig. 18. Dynamic performance of the EPI when programmed from a linear capacitor to a frequency-dependent capacitor under the condition of (a) i_{dis} having a frequency of 50 Hz and (b) i_{dis} having a frequency of 100 Hz.

A plug-and-play ripple mitigator is a device which has a low impedance only at selective frequencies while it has an infinitely large impedance at DC [17]. This can be achieved by programming the EPI as a frequency-dependent capacitor, i.e., configuring $G(s)$ in Fig. 12 into an R function. To demonstrate the frequency-dependent V-I characteristics of the EPI, two similar experiments are conducted and the results are shown in Fig. 18. In both experiments, $G(s)$ is changed from an R function ($G(s)$ =

$\frac{20\times(2\times\pi\times10)s}{s^2+(2\times\pi\times10)s+(2\times\pi\times50)^2}$) to a *P* function (*G*(*s*) = 20) to. The frequency of the disturbing current i_{dis} is set at 50 Hz and 100 Hz in Fig. 18 (a) and (b), respectively. Based on the *R* and the *P* function configured, the EPI is always emulating a 210 μF capacitor at 50 Hz (11 times of amplification of C_o) before and after the step change. Therefore, the waveforms of v_f, i_f and v_c remains in Fig. 18 (a) when the type of the impedance is changed. At 100 Hz, however, the filtering effect of the EPI based on the *R* and the *P* function becomes different, as clearly indicated Fig. 18(b). These results confirm that an EPI based on an *R* function has a frequency-dependent capacitance value. The results also demonstrate that a fast changing between an emulated linear capacitor and a frequency-dependent capacitor is viable.

3) *EPI as a Negative Capacitor (Changing G(s) from P Function to –P Function)*

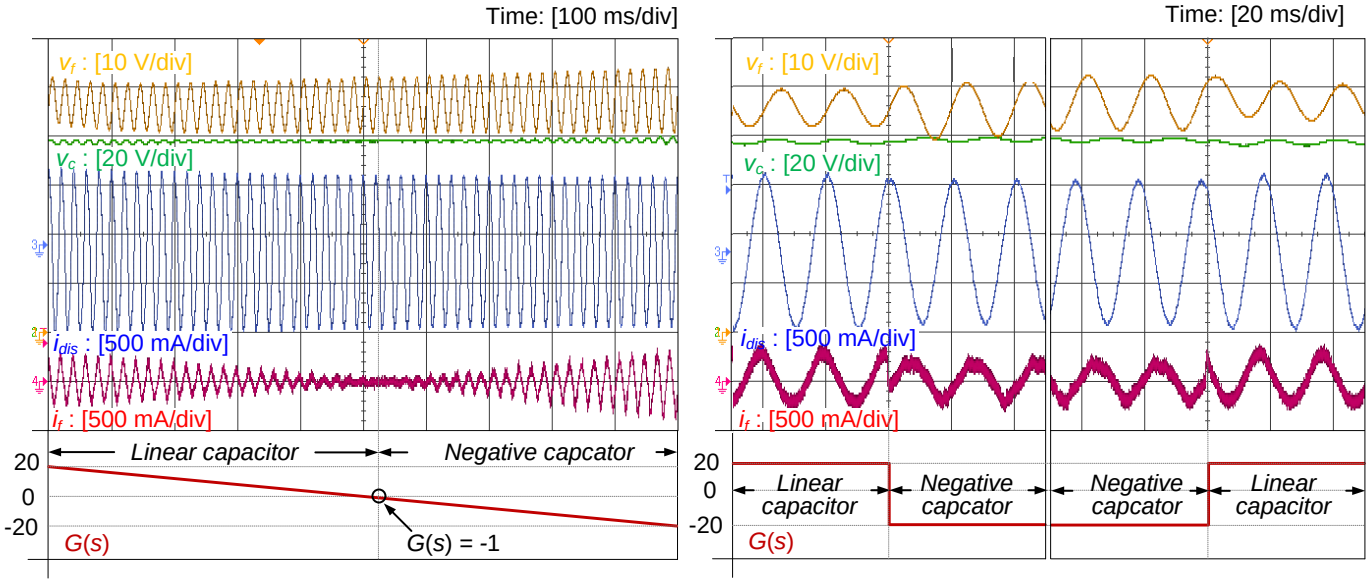

(a) (b)

Fig. 19. Dynamic performance of the EPI when programmed from a linear capacitor to a negative capacitor. The capacitance value is changed smoothly in (a) and is step changed in (b) from 210 μF to −190 μF.

A negative capacitor can be achieved by configuring *G*(*s*) as a *–P* function. In this experiment, an extra DC capacitor of 200 μF is connected in shunt with the load R_o (not shown in Fig. 12) to test the performance of a negative capacitor. The use of the extra capacitor in the system is to ensure a positive overall capacitance

in the system in order to guarantee stable system operation. The reason is analogue to that explained in [14] for a negative inductor.

When $G(s)$ is smoothly changing from 20 to −20 as shown in Fig. 19, the EPI is emulating a capacitor with a capacitance value between 210 μF to −190 μF. Considering the extra added 200 μF capacitor, the total capacitance value of the DC system varies between 410 μF to 10 μF. As the total capacitance of the DC system decreases, the amplitude of v_f increases. An interesting phenomenon can be observed before and after $G(s)$ passes the negative unity gain point (i.e., $G(s) = -1$): i_f is leading the AC portion of v_f by 90° when $G(s) > -1$ and i_f is lagging the AC portion of v_f by 90° when $G(s) < -1$. These results show that a negative capacitor has the same steady-state V-I characteristics as an inductor. In Fig. 19(b), a test of step change of $G(s)$ between 20 to −20 is conducted. It can be seen that fast transition between a linear capacitor and a negative capacitor has been achieved.

4) EPI as a Static Var Compensator (Changing G(s) from R Function to −R Function)

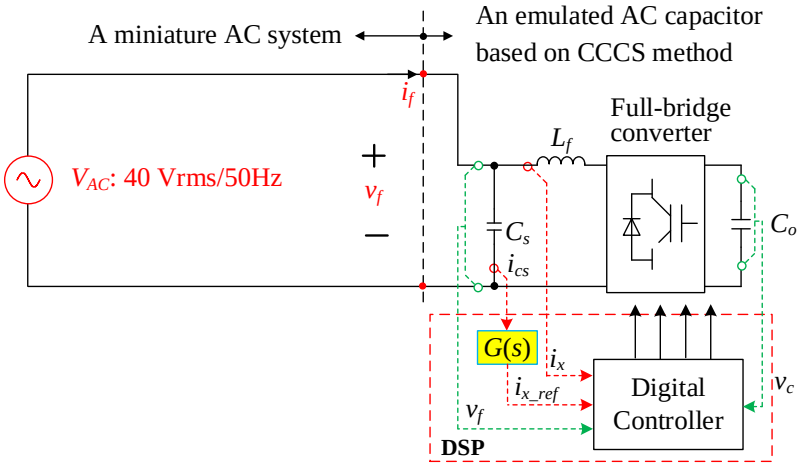

Fig. 20. Experiment setup for testing the dynamic perfirmance of an EPI as a Static Var Compensator.

An SVC can be regarded as a type of dynamic frequency-dependent reactance, of which both inductive and capacitive reactive power generation needs to be generated. To achieve reactive power generation for a 50 Hz system, $G(s)$ is set as an R function ($\frac{(2\times\pi\times10)s}{s^2+(2\times\pi\times10)s+(2\times\pi\times50)^2}$) which has a unity gain at 50 Hz. Variable capacitive power generation can be achieved by configuring the gain of the R function to be larger

than −1, whereas inductive power generation can be achieved when the gain of the *R* function is less than −1. A miniature 20 Vrms/ 50 Hz AC system powered by an AC voltage source V_{AC} is used to test the performance of the EPI (Fig. 20). Note that the hardware of the EPI is identical to that used in Fig. 12. Fig. 21 shows the measured v_f, i_f and the instantaneous reactive power when the gain of the *R* function changes between 20 and −20.

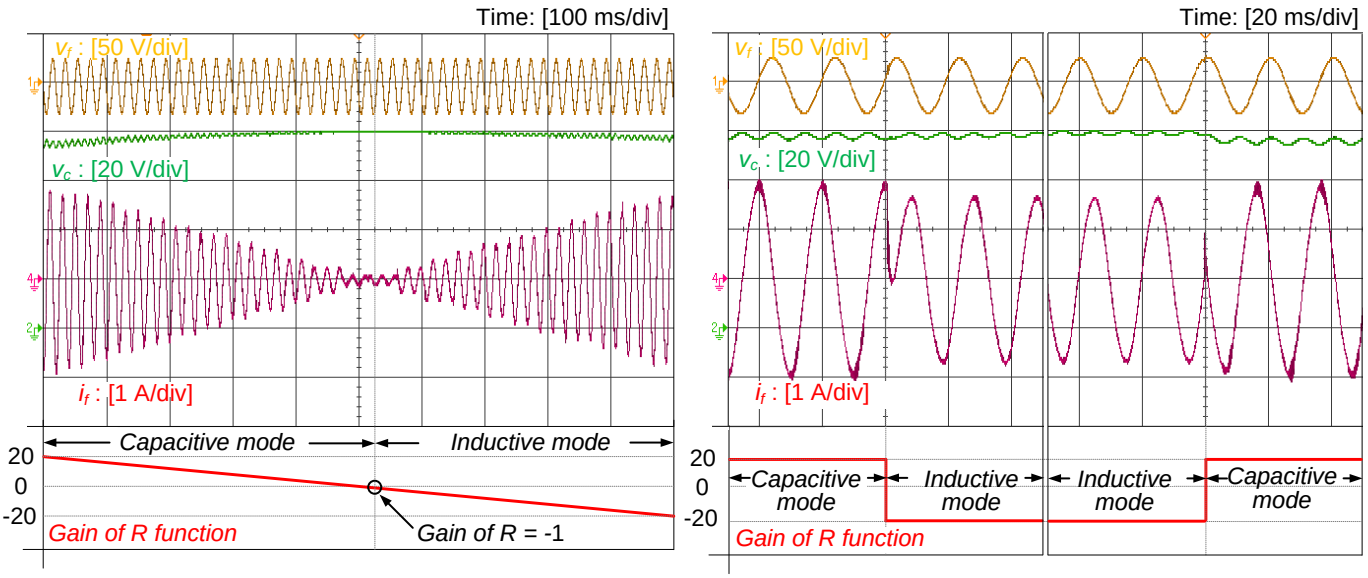

(a) (b)

Fig. 21. Dynamic performance of the EPI when changed from a frequency-dependent capacitor to a frequency-dependent inductor. The gain of the *R* function is changed smoothly in (a) and is step changed in (b) between 10 to −10.

It can be seen from Fig. 21(a) that, as the gain of the *R* function passes the −1 point, the phase relationship between i_f and v_f also changes from leading 90° to lagging 90°. It can also be observed that, as the gain of *R* gradually reduces, the reactive current i_f and hence the produced reactive power changes linearly and seamlessly.

A step change of *G*(*s*) between capacitive and inductive mode of operation is performed and shown in Fig. 21(b). When the gain of the *R* function is step changed from 20 to −20 or inversely, the phase of i_f with respect to v_f is changed instantly. Therefore, fast switching between a frequency-dependent capacitor/inductor has been demonstrated. The results also indicate that a fast dynamic SVC based on direct impedance control is feasible.

VI. CONCLUSIONS

In this paper, a general control strategy for actuating a programmable and re-configurable power impedance is presented. The challenges, control method and practical considerations are explained. A programmable power reactance which can be configured as a linear capacitor, a negative capacitor, a frequency-dependent capacitor or a frequency-dependent inductor, has been successfully demonstrated and tested in hardware using a full-bridge inverter with small passive reactive components. With the proposed control method, fast changing between different reactance values and types is feasible. The control method can be further extended to emulate a general form of power impedance provided that the power converter is capable of both real and reactive power generation. Unlike existing EPIs which are designed specifically for a single task, the programmable EPI here can achieve multiple functions according to the user input. The concept of programmable EPI may offer a new and flexible way to perform power filtering, energy storage and even power conversion from an impedance perspective.

REFERENCES

[1] Power Electronics Group, “Input-current shaped AC-to-DC converters,” in *Final Report Prepared for NASA*, 1986.

[2] H. Funato and A. Kawamura, “Proposal of variable active-passive reactance,” in *International Conference on Industrial Electronics, Control, Instrumentation, and Automation*, 1992, pp. 381–388.

[3] O. Kirshenboim, A. Cervera, B. Halivni, E. Abramov, and M. M. Peretz, “Plug-and-Play Electronic Capacitor for VRM Applications,” in *IEEE Applied Power Electronics Conference and Exposition*, 2016, pp. 111–117.

[4] D. Rana, B. Hafez, P. Garg, S. Essakiappan, and P. Enjeti, “Analysis and design of active inductor as DC-link reactor for lightweight adjustable speed drive systems,” in *IEEE Energy Conversion Congress and Exposition*, 2014, pp. 3243–3250.

[5] C. C. Yang, Y. L. Chen, and Y. M. Chen, “Active capacitor with ripple-based duty cycle modulation for AC-DC applications,” in *IEEE Applied Power Electronics Conference and Exposition*, 2016, pp. 558–563.

[6] S.-Y. Lee, Y.-L. Chen, Y.-M. Chen, and K. H. Liu, “Development of the active capacitor for PFC converters,” in *IEEE Energy Conversion Congress and Exposition*, 2014, pp. 1522–1527.

[7] B. Liu, S. Zhang, S. Zheng, Y. Ma, F. Wang, and L. M. Tolbert, “Design consideration of converter based transmission line emulation,” in *IEEE Applied Power Electronics Conference and Exposition*, 2016, pp. 966–973.

[8] X. Zhang, X. Ruan, H. Kim, and C. K. Tse, “Adaptive active capacitor converter for improving stability of cascaded DC power supply system,” *IEEE Trans. Power Electron.*, vol. 28, no. 4, pp. 1807–1816, Apr. 2013.

[9] X. Chen, K. Dai, C. Xu, Z. Dai, and L. Peng, “Reactive power compensation with improvement of current waveform quality for single-phase buck-type Dynamic Capacitor,” in *IEEE Applied Power Electronics Conference and Exposition*, 2016, pp. 1358–1363.

[10] S. Inoue, T. Shimizu, and K. Wada, “Control Methods and Compensation Characteristics of a Series Active Filter for a Neutral Conductor,” *IEEE Trans. Ind. Electron.*, vol. 54, no. 1, pp. 433–440, Feb. 2007.

[11] A. Nabae, Y. Nakajima, L. Cao, T. Tanaka, and S. Ariga, “A series active capacitance for compensating voltage drops caused by source impedances in power systems,” in *IEEE Power Electronics Specialists Conference*, 1997, vol. 1, pp. 351–355.

[12] J. C. P. Liu, C. K. Tse, F. N. K. Poon, M. H. Pong, and Y. M. Lai, in *International journal of circuit theory and applications*, 2008, v. 36, no. 3, p. 275-287.

[13] B. Liu, S. Zheng, Y. Ma, F. Wang, and L. M. Tolbert, “Control and implementation of converter based ac transmission line emulation,” in *IEEE Applied Power Electronics Conference and Exposition*, 2015, pp. 1807–1814.

[14] H. Funato, A. Kawamura, and K. Kamiyama, “Realization of negative inductance using variable active-passive reactance (VAPAR),” *IEEE Trans. Power Electron.*, vol. 12, no. 4, pp. 589–596, Jul. 1997.

[15] S. Wang, X. Ruan, K. Yao, S.-C. Tan, Y. Yang, and Z. Ye, “A flicker-free electrolytic capacitor-less AC–DC LED driver,” *IEEE Trans. Power Electron.*, vol. 27, no. 11, pp. 4540–4548, Nov. 2012.

[16] W. Qi, H. Wang, X. Tan, G. Wang, and K. D. T. Ngo, “A novel active power decoupling single-phase PWM rectifier topology,” in *IEEE Applied Power Electronics Conference and Exposition*, 2014, pp. 89–95.

[17] S. Li, A. T. L. Lee, S. C. Tan, and S. Y. R. Hui, “A Plug-and-Play Ripple Mitigation Approach for DC-Links in Hybrid Systems,” in *Applied Power Electronics Conference and Exposition*, 2016, pp. 169 – 176.